JOURNAL OF MAGNETIC RESONANCE **126,** 159–163 (1997)
ARTICLE NO. MN971150

Slow Dynamics Mapping of Large-Linewidth Solids by a MARF Spin-Lock Filter

F. De Luca, G. H. Raza, A. Gargaro, and B. Maraviglia

Dipartimento di Fisica, Universitá ''La Sapienza,'' 00185 Rome, Italy

Received July 31, 1996; revised February 21, 1997

A new method for $T_{1\rho}$ contrast in solid-state imaging is presented. The method is based upon the addition of a $T_{1\rho}$ spin-lock pulse to the standard MARF pulse sequence and is able to provide relaxation contrast in dependence either on the lock time or on the intensity of the lock field, without having effects related to the line-narrowing procedure. The results on some large-linewidth solids show that $T_{1\rho}$ values measured by the usual spin-lock pulse sequence agree with those measured on space-resolved lines. © 1997 Academic Press

INTRODUCTION

During the past several years, several methods for NMR imaging of large-linewidth samples have been developed (*1–7*). These methods, with more or less experimental complications, are able to provide a spatial ''portrait'' of solid samples by means of NMR parameters, ranging from local equilibrium magnetization to specialized relaxation times (*8*), that is through observables which provide information on the structure and on the dynamical process characteristics of the solid. It is to be expected that such a wide availability of localized information could make the solid-state imaging competitive with respect to the higher-resolution microscopy techniques.

The most promising NMR-imaging approaches (*9*), which stand for an easy-handling contrast of solid samples, utilize some line-narrowing devices to facilitate spatial encoding. The timing scheme of the pulse sequence, which applies to such *c*oherent *a*veraging-assisted *s*olid-state *i*maging (CASSI) methods, follows a quite standard scheme made up of three main periods: an early period (filter period), in which the magnetization is manipulated so that its amplitude is influenced by some NMR parameters; a successive period (space-encoding period), during which the line narrowing and the space encoding are performed; and a final period (detection period), where the spectroscopic detection of the NMR signal is fulfilled (*10, 11*). A frequent consequence of such a scheme is the influence (not yet adequately recognized) of the line narrowing on the CASSI contrast planned in the filter period. Even if this effect may produce unconventional NMR parameter maps of some practical utilization (*12*), in general, care must be taken when a microscopic interpretation is attempted by means of contrast parameters appearing on images obtained with CASSI methods.

These considerations are to some extent crucial to CASSI, whose filter period aims to obtain contrast in $T_{1\rho}$, the relaxation time in the rotating frame (*13*). As is well known, $T_{1\rho}$ accounts for molecular motion, whose spectral density falls in the effective frequency range (typically 1–200 kHz), that is, for motion with correlation times longer than those detectable via T_1 (*14*). Since the molecular motion in elastomers, entangled polymers, macromolecular aggregates, etc., is particularly active in that frequency range, $T_{1\rho}$ is peculiarly suitable for contrast in CASSI (*15*). The $T_{1\rho}$ filter has been applied to CASSI by following the strategy outlined above: a spin-lock pulse precedes (sometimes is incorporated in) the space-encoding period (*6, 11, 16*) and the $T_{1\rho}$ influence on the image contrast is controlled by the lock-time length.

Our approach to CASSI is based on the spin-space parameter dependence that spin interactions assume in the various reference frames where the spin Hamiltonians can be represented. In particular, in the tilted rotating frame (in this frame the Zeeman axis coincides with the effective field direction), the coherent averaging condition, the so-called magic-angle condition (*17, 18*), consists of a definite relation between the radiofrequency field intensity B_1 and the resonance offset $\Delta\omega$. MARF imaging [discussed exhaustively in several papers (*19*)], besides the back-projection and the 2DFT opportunities (*20*) together with the slice-selection capability (*21*), allows one to get image contrast without the influence of the narrowing condition (*19*). In other words, the image-contrast filter is applied after the spatial-encoding period. In fact, before detection, the space-encoded magnetization is stored as longitudinal magnetization and can be handled, in principle, by every pulse sequence. The cost of such an advantage is that the detection of the complete evolution of the magnetization in the tilted rotating frame must be made step-by-step (*22*).

In this paper we present a simple and effective improvement of the MARF imaging method that allows one to filter the space-encoded magnetization by only $T_{1\rho}$. The filter,

1090-7807/97 $25.00
Copyright © 1997 by Academic Press
All rights of reproduction in any form reserved.

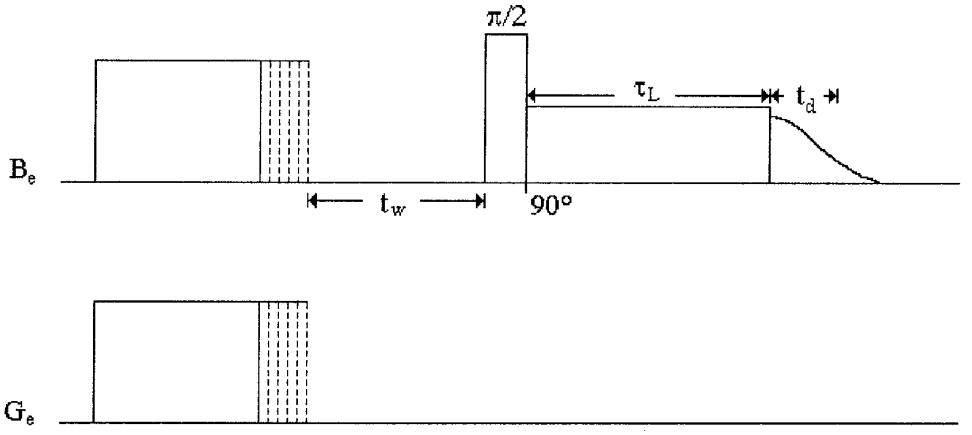

FIG. 1. Timing diagram of the $T_{1\rho}$ filter MARF imaging sequence. For the sake of simplicity, the effective field B_e and the effective gradient G_e, which are given by the superposition of static and radiofrequency fields, are divided just into two lines. The on-resonance $\pi/2$ pulse tilts the space-encoded longitudinal magnetization on the transverse plane while the 90° phase-shifted spin-lock pulse locks the magnetization along the B_1 direction for a time τ_L. While the filtering sequence and the signal detection are performed on resonance, the space-encoding sequence is off resonance to match the magic-angle condition. The vertical dashed lines indicate the stepping of both the effective field and the effective gradient that allows step-by-step reconstruction of the magnetization evolution around the effective field. The time t_w must be greater than the longer full transverse relaxation time of the sample. In our case it is fixed at a value of about 25 ms which also matches the condition $t_w \ll T_1$, where T_1 is the shorter longitudinal relaxation time of the sample. The delayed sampling time t_d allows the inclusion of linewidth contrast in the postprocessing of the experimental data.

made by a spin-lock pulse added to a standard MARF imaging sequence (Fig. 1), yields a ''pure'' $T_{1\rho}(r)$ contrast, as a function either of the lock time τ_L or of the intensity of the lock field B_1.

RESULTS

A $T_{1\rho}(r)$-filtered MARF profile is acquired by detecting the FID amplitude at $t_d \cong 0$ (Fig. 1) for each step of the effective field and gradient, with which the relaxation of transverse magnetization in the tilted rotating frame is sampled. The spin-lock pulse attenuates the FID by a factor $\exp\{-\tau_L/T_{1\rho}(r)\}$ and modulates the spatial profile according to $T_{1\rho}(r)$. If the sampling point of the FID is delayed by $t_d \neq 0$, the $T_{1\rho}(r)$-filtered MARF signal is also influenced by the sample linewidth.

The efficacy of the $T_{1\rho}$ filter has been tested on a phantom composed of Delrin (polyacetal), Vetronite (polyether resin reinforced by glass textile), and adamantane (Fig. 2). Delrin and adamantane linewidths are about 20 kHz while the Vetronite linewidth is about 50 kHz.

All measurements have been performed on a modified Bruker SXP spectrometer operating with a 0.7 T electromagnet. The coil assembly is formed of a surface coil, which produces the radiofrequency gradient and field (*23*), and of a solenoidal coil which produces the $\pi/2$ and lock pulses. The magnetic axes of the two coils are orthogonal to minimize the mutual coupling. The coil set is completed by a gradient coil which generates the static field gradient that makes the magic-angle condition independent of the sample extension (*17*). Under our experimental conditions, the surface coil produces a field of about 1.7 mT, which, combined with a resonance offset of about 1.2 mT, gives an effective field of about 2.1 mT, and a radiofrequency gradient of about 60 mT/m. This last gradient combined with the static gradient of about 43 mT/m allows a spatial resolution of

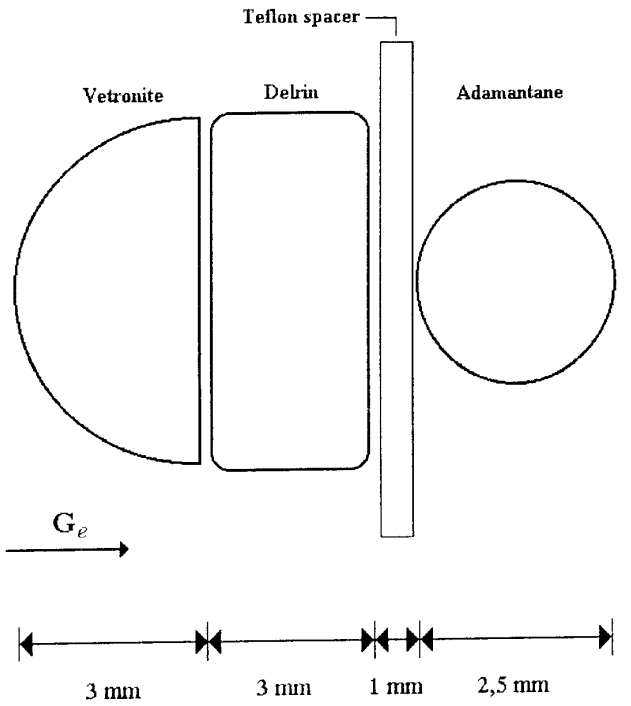

FIG. 2. Sketch of the phantom used to test the sequence of Fig. 1. Adamantane powder was contained in a glass tube, so a wall thickness of 0.5 mm must be considered. All the samples have axial symmetry and their lengths are about 6 mm.

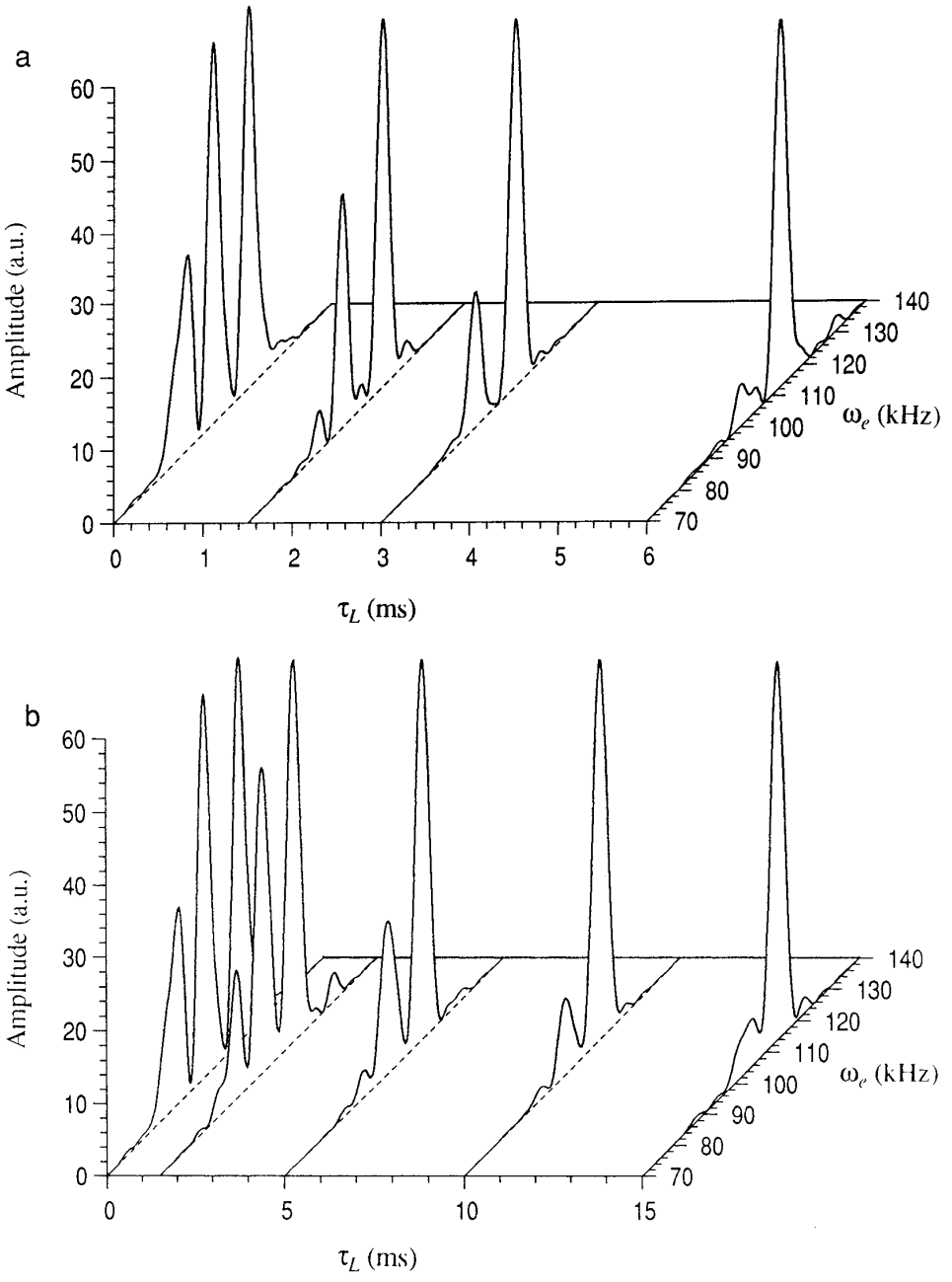

FIG. 3. Results of the sequence of Fig. 1 on the sample of Fig. 2 for different spin-lock pulse lengths τ_L. The spin-lock field intensity is about 0.38 mT in (3a) and about 0.94 mT in (3b). The adamantane peaks are those at the higher effective frequencies. Each profile has been averaged three times.

about 300 μm. The resolution is independent of sample linewidths because the well-established condition $[(\gamma B_1)^2 + \Delta\omega^2]^{1/2} \gg \Delta\Omega$ (where $\Delta\Omega$ is the maximum sample linewidth and γ the gyromagnetic ratio) makes the line narrowing limited only by the radiofrequency field and static magnetic field inhomogeneity (*24*).

In Figs. 3a and 3b, the $T_{1\rho}$-filtered profiles of the phantom at different lock times and field intensities are reported for $t_d \cong 0$. In Figs. 3a and 3b the lock field intensities are about 0.38 and 0.94 mT, respectively. According to their $T_{1\rho}$ values, the adamantane and Delrin profiles are effectively differentiated and the Vetronite peak disappears already at $\tau_L \cong 5$ ms. The contrast enhancement is rather dramatic with respect to the $\tau_L \cong 0$ profile, especially between Delrin and adamantane, whose linewidths are similar. The small difference between the profiles of Figs. 3a and 3b (as well as in the $T_{1\rho}$ data) is probably due to the restricted range of the effective frequency that we can explore with our electronics.

In Fig. 4 the amplitudes of the three peaks of Fig. 3a vs

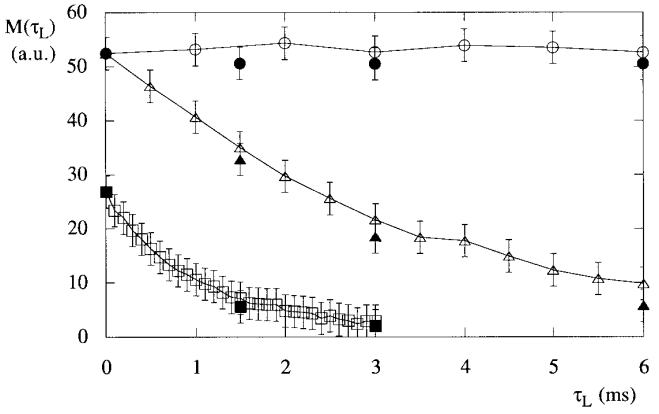

FIG. 4. This figure presents the comparison between $T_{1\rho}$ measured with the usual spin-lock pulse sequence on each material of the phantom of Fig. 2 and the peak amplitudes of Fig. 3a. In both cases the lock field intensity was 0.38 mT. The circles refer to adamantane, the triangles to Delrin, and the squares to Vetronite. The solid symbols indicate the peak amplitudes of Fig. 3a while the open symbols indicate the magnetization measured for different values of τ_L. The peak amplitudes are normalized so that the peaks at $\tau_L = 0$ correspond to the proper sample magnetization at $\tau_L = 0$. The solid lines are a guide to the eye.

τ_L and the magnetization amplitudes of each material of Fig. 2 acquired at the same lock field by a standard spin-lock sequence (*25*) are compared at the same lock times. As can be seen, the data match fully, within the experimental errors, showing that the contrast obtained through the sequence of Fig. 1 is produced only by the $T_{1\rho}$ of the three materials, namely that the magnetization-filtering procedure of the sequence of Fig. 1 is independent of the spatial-encoding procedure. The same conclusion can be reached by comparing the experimental results obtained with a lock field intensity of 0.94 mT and the profiles of Fig. 3b. For this effective field intensity we get the following experimental values for $T_{1\rho}$: adamantane $T_{1\rho} > 60$ ms, Delrin $T_{1\rho} = 8.0 \pm 0.3$ ms, and Vetronite $T_{1\rho} = 1.8 \pm 0.1$ ms.

As an example of the versatility of the sequence reported in Fig. 1, the data of Fig. 3b with $\tau_L \cong 5$ ms are processed for different values of t_d and reported in Fig. 5. In this way, a bandwidth contribution is mixed to the $T_{1\rho}$ contrast without the need for new experimental data. The Vetronite peak, thanks to its large linewidth and short $T_{1\rho}$, disappears rapidly while the Delrin and adamantane peaks tend to equalize under the effect of their similar linewidths. The manipulation of the contrast without time-consuming experiments could be useful in those situations where a qualitative contrast is required or in those experimental situations that are intrinsically poorly reproducible (as, for example, in stretched elastomers).

In this paper, we have presented a new method for obtaining $T_{1\rho}$ contrast in CASSI of very large-linewidth systems. This method permits good spatial resolution and very effective $T_{1\rho}$ contrast with a tolerable loss in the signal-to-noise ratio. The $T_{1\rho}$ contrast obtained with the sequence of Fig. 1 is ''quantitative'' in the sense that it depends on only $T_{1\rho}$ and that neither the spatial encoding nor the narrowing sequence affects it.

In broad-line spin systems, $T_{1\rho}(r)$ sensitivity may lead to very useful information, since it may be related to the low-frequency molecular motion (*26, 27*), which in solid samples is quite an important dynamics component. Slow dy-

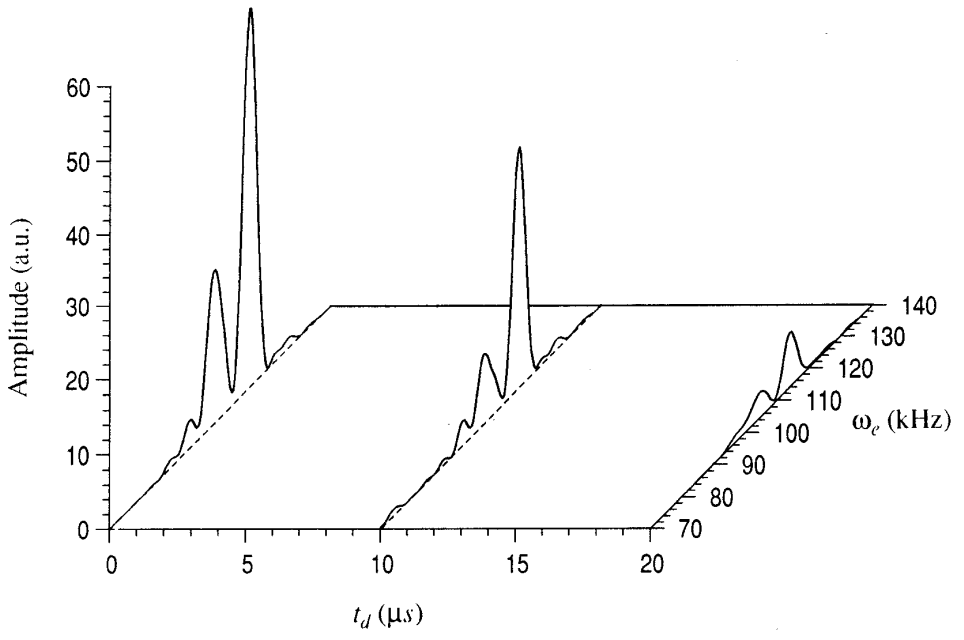

FIG. 5. Several projections obtained by including the effect of the delayed sampling time t_d. The data of the profile with $\tau_L = 5$ ms of Fig. 3b are processed with different values of t_d.

namics is expected in fact to be sensitive to the main macroscopic stresses, like mechanical, thermal, or manufacturing-induced stresses, that usually affect solids.

REFERENCES

1. A. N. Garroway, J. Baum, M. G. Munowitz, and A. Pines, *J. Magn. Reson.* **60,** 337 (1984).
2. A. A. Samoilenko, D. Yu Artemov, and L. A. Sibel'dina, *JEPT Lett.* **47,** 477 (1988).
3. D. G. Cory, J. B. Miller, and A. N. Garroway, *J. Magn. Reson.* **90,** 205 (1990).
4. R. Kimmich, D. E. Demco, and S. Hafner, *in* ''Magnetic Resonance Microscopy,'' p. 59, VCH, Weinheim, 1992.
5. M. L. Buszko and G. E. Maciel, *J. Magn. Reson. A* **107,** 151 (1994).
6. P. Barth, S. Hafner, and W. Kuhn, *J. Magn. Reson. A* **110,** 198 (1994).
7. S. Matsui, A. Uraoka, and T. Inouye, *J. Magn. Reson. A* **120,** 11 (1996).
8. K. Schmidt-Rohr and H. W. Spiess, ''Multidimensional Solid-State NMR and Polymers,'' Academic Press, San Diego, 1994.
9. P. Barth, S. Hafner, and W. Kuhn, *J. Magn. Reson. A* **110,** 198 (1994).
10. F. Weigand, D. E. Demco, B. Blumich, and H. W. Spiess, *J. Magn. Reson. A* **120,** 190 (1996).
11. P. Blümler and B. Blümich, *Magn. Reson. Imaging* **10,** 779 (1992).
12. F. Weigand and H. S. Spiess, *Macromolecules* **28,** 6361 (1995).
13. A. G. Redfield, *Phys. Rev. Lett.* **98,** 1787 (1955).
14. D. C. Ailion, *Adv. Magn. Reson.,* Suppl. 2 (1982).
15. W. Kuhn, E. Koeller, and I. Theis, *in* ''Magnetic Resonance Microscopy,'' p. 217, VCH, V Weinheim, 1992.
16. G. C. Chingas, J. B. Miller, and A. N. Garroway, *J. Magn. Reson.* **66,** 530 (1986).
17. F. De Luca, N. Lugeri, B. C. De Simone, and B. Maraviglia, *Solid State Commun.* **82,** 151 (1992).
18. M. Lee and W. I. Goldburg, *Phys. Rev. Lett.* **11,** 255 (1965).
19. F. De Luca, N. Lugeri, S. Motta, G. Cammisa, and B. Maraviglia, *J. Magn. Reson. A* **115,** 1 (1995).
20. F. De Luca, N. Lugeri, B. C. De Simone, and B. Maraviglia, *Colloids Surf.* **72,** 63 (1993).
21. F. De Luca, N. Lugeri, S. Motta, and B. Maraviglia, *J. Magn. Reson. A* **121,** 114 (1996).
22. F. De Luca, B. C. De Simone, N. Lugeri, and B. Maraviglia, *J. Magn. Reson. A* **107,** 243 (1994).
23. D. Boudot, D. Canet, and J. Brondeau, *J. Magn. Reson.* **87,** 385 (1990).
24. M. Lee and W. I. Goldburg, *Phys. Rev. A* **140,** 1261 (1965).
25. C. P. Slichter, ''Principles of Magnetic Resonance,'' Springer-Verlag, Berlin/Heidelberg, 1990.
26. D. Wolf, ''Spin-Temperature and Nuclear-Spin Relaxation in Matter,'' Oxford Univ. Press, New York, 1979.
27. N. Fatkullin and R. Kimmich, *J. Chem. Phys.* **101**(1), 822 (1994).